The International Journal of Advanced Manufacturing Technology (2018) 96:451–460
https://doi.org/10.1007/s00170-018-1591-z

ORIGINAL ARTICLE

Uniform concentrating design and mold machining of Fresnel lens for photovoltaic systems

Xing Gao [1,2] · Yong Li [1,2] · Quancun Kong [1,2,3] · Qifeng Tan [1,2] · Chaojiang Li [1,2]

Received: 4 April 2017 / Accepted: 9 January 2018 / Published online: 23 January 2018

Abstract
Fresnel lens arrays are widely applied as the core optical component in concentrated photovoltaic (CPV) systems for concentrating light on a solar cell. To improve the photoelectric conversion efficiency of CPV systems, a Fresnel lens design is proposed, in which both uniform concentration and machining feasibility are pursued by means of simpler structure. In this design, the concentrating facets of the Fresnel lens are conical ones with different inclined angles, and the light passing through these conical facets can be superposed on the same position. The optical performance of the lens is analyzed to optimize its geometrical parameters. Towards this uniform concentrating design with a simple structure, an ultra-precision diamond cutting process based on *B* axis rotation is also developed to machine the Fresnel lens mold. In this process, the V-shaped diamond tool is rotated from right to left to machine the micro grooves of the lens mold with a maximum cutting depth of the groove height, so that the grooves can be prevented from being cut by the tool tip with low strength. Cutting tests of the factors influencing the machining accuracy and surface quality are carried out to optimize the cutting trajectory planning and machining parameters. The Fresnel lens molds with no sharp corner defects and no surface scratches are machined, and dimensional accuracy of 1.0 μm and surface roughness of better than 13 nm are achieved. Then, a silicone rubber lens is cast based on this mold. Concentrating uniformity test of the lens is conducted, and a concentrating uniformity of better than 75% is achieved. The results show the effectiveness of the uniform concentrating design and the feasibility of the *B* axis rotating machining process.

Keywords Concentrated photovoltaic (CPV) systems · Uniform concentration · Fresnel lens and its mold · Ultra-precision cutting · *B* axis rotating machining

1 Introduction

The photoelectric conversion efficiency of concentrated photovoltaic (CPV) technology is more than 30%, which has a great development potential [1, 2]. In CPV system, Fresnel lenses are used as light concentrators, which directly affect the photoelectric conversion efficiency. However, the traditional Fresnel lens generates a hot spot on a solar cell, which will decrease the photoelectric conversion efficiency and reliability of the solar cell [3, 4]. A secondary optical component (SOC) [5, 6] between the lens and the solar cell must be used for uniform energy distribution. The SOC will increase the cost, loss of light, and complexity of CPV system. Thus, the design of a uniform concentrating Fresnel lens without SOC is an important issue in CPV field [6].

Up to now, the optimal design of traditional Fresnel lens has been conducted to achieve uniform energy distribution. In 2011, a uniform high-concentrating Fresnel lens without a SOC was proposed [7], of which all pitches focused on the different positions of the cell. All the inclined angles of these pitches were determined by specific calculation. The simulation results showed that a better uniform concentration was achieved. Uniform concentration test was not carried out to verify the simulation results. In 2012, a strip-focus Fresnel concentrator without a SOC was proposed [8]. The simulation results indicated the strip-focus Fresnel lens had a higher

✉ Yong Li
liyong@mail.tsinghua.edu.cn

[1] Beijing Key Lab of Precision/Ultra-precision Manufacturing Equipments of Control, Department of Mechanical Engineering, Tsinghua University, Beijing 100084, China

[2] State Key Laboratory of Tribology, Tsinghua University, Beijing 100084, China

[3] School of Instrumentation Science and Opto-Electronics Engineering, Beijing Information Science and Technology University, Beijing 100192, China

uniformity and efficiency. The strip-focus structure could not be easily cut. Machining and uniform concentration verification of the strip-focus concentrator were not carried out. Different kinds of Fresnel lenses, such as the strip-focus and circle-focus ones, have been designed for uniform concentration, but there is lack of machining and uniform concentration verification. Moreover, these lenses usually have a complex structure and are difficult to be machined.

Mass production of Fresnel lens arrays for CPV system is conducted via its precision optical mold with micron-scale dimensional accuracy, nano-scale surface roughness, and complex aspheric cavity. Optical surface can be achieved by grinding and polishing, but the complex aspheric cavity is difficult to be machined by these ways [9, 10]. At present, the Fresnel lens and its mold are mostly machined by ultra-precision cutting technology. In 2005, an infrared Fresnel lens with dimensional accuracy of 0.5 μm and surface roughness Ry of 20–50 nm was ultra-precision cut on single-crystal germanium [11]. In 2010, an ultra-precision cutting process of Fresnel lens was proposed [12] to prevent the micro crack of the groove edge. The lens was cut by the tool with multi-motion of X and Z axes, while the tool was rotated simultaneously to ensure a constant cutting edge angle. The tool tip was mainly engaged in the cutting process. The cutting depth was 50 μm. In 2011, an ultra-precision cutting method of Fresnel lens mold was proposed [13] to reduce the loss of light. The non-working surface of the mold was machined by multiple cuts to ensure the sharp corner of the groove. In 2011, a plasma nitriding die steel Fresnel lens was machined based on ultra-precision cutting [14]. The same cutting process in [12] was applied, and the cutting depth was also 50 μm. In 2014 and 2015, a B axis rotation tool alignment method was proposed by us [15, 16], in which the alignment accuracy was less than 1 μm. A spot-focus Fresnel lens mold without uniform concentration was designed and machined by multiple cuts. Optical surface of the mold was achieved, but there were obvious burrs and sharp corner defects in the groove of this machined mold.

But above all, burrs, sharp corner defects, or surface scratches are easily induced in the process of ultra-precision cutting Fresnel lens [17], which will decrease the photoelectric conversion efficiency. More attention should be paid to preventing these machining defects, and meanwhile to improving the machining efficiency.

In this paper, a uniform concentrating design of Fresnel lens without a SOC is proposed, in which the machining feasibility of Fresnel lens mold is considered. By analyzing factors influencing the ideal optical efficiency and optical concentrating ratio, the geometrical parameters of the lens are optimized. Then, an ultra-precision cutting process of the lens mold based on the B axis rotation method in [15] is developed to improve the machining efficiency. The cutting trajectory planning and machining parameters are optimized through cutting tests to prevent burrs, sharp corner defects, or surface scratches. Finally, machining experiments of the Fresnel lens mold and the concentrating uniformity test of the lens are carried out.

2 Design of uniform concentrating Fresnel lens

2.1 Uniform concentrating principle

Figure 1 shows the uniform concentrating principle. The light passing through the Fresnel lens facets focuses on a circular facula with a specific diameter. Normal incident light passes through the lens and is refracted, but keeps parallel to each other. Consequently, the refracted light from different grooves with equal width can be superposed in the same area with uniform energy distribution [8].

The diameter of the solar cell equals to that of the concentrating facula, defined as l. The lens consists of a center circle surface and certain grooves. To ensure that the refracted light from different grooves is superposed in the same area, the diameter of the center circular surface and the width of the grooves must equal to l and $l/2$ respectively. To reduce the thickness of the lens, every groove is subdivided into certain smaller grooves with the same inclined angle. Figure 2 shows the light path of single groove. The refractive index and the inclined angle of single groove are defined as n and θ respectively. The incident angle and the refraction angle at O_1 are defined as γ_1 and γ_2 respectively, and those at O_2 are defined as φ_1 and φ_2 respectively. The included angle between the incident ray and the emergent ray is defined as α. According to Snell's law, the relationship among γ_1, γ_2, φ_1, and φ_2 is described in Eq. 1.

$$\sin\gamma_1/\sin\gamma_2 = \sin\varphi_2/\sin\varphi_1 = n \tag{1}$$

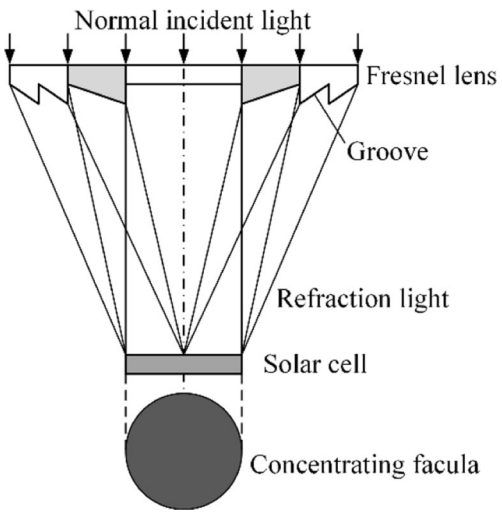

Fig. 1 Uniform concentrating principle

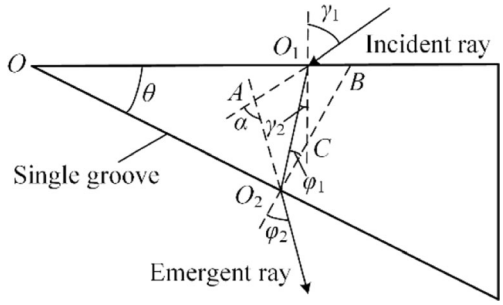

Fig. 2 Light path of single pitch

According to the geometrical relationship of single groove, the relationship among γ_1, γ_2, φ_1, φ_2, and θ can be described in Eq. 2.

$$\varphi_1 = \theta - \gamma_2, \alpha = \gamma_1 + \varphi_2 - \theta \tag{2}$$

When the lens works, normal incident light is needed and thus $\gamma_1 = 0°$. According to Eqs. 1 and 2, the relationship between α and θ is described in Eq. 3.

$$\theta = \tan^{-1}[\sin\alpha/(n - \cos\alpha)] \tag{3}$$

2.2 Optical design

As shown in Fig. 3, f is the focal length of the uniform concentrating Fresnel lens, and d is the diameter of the lens which consists of M grooves. N is the groove number from the middle to the left. $N = d/l$, and $M = 2N - 1$, and j is the number of an arbitrary groove. According to Eq. 3, the relationship between α and θ can be described in Eq. 4.

$$\alpha_j = \tan^{-1}[(j-1)l/(2f)], \quad \theta_j = \tan^{-1}\left[\sin\alpha_j/\left(n - \cos\alpha_j\right)\right] \tag{4}$$

h_j and d_j are the height and the width of the number j groove respectively. Every groove is divided into m sub-grooves. h_j and d_j can be calculated by Eq. 5. Finally, the geometrical parameters of the lens are totally defined by Eqs. 4 and 5.

$$d_j = h_j/\tan\theta_j, \quad m = l/2d_j \tag{5}$$

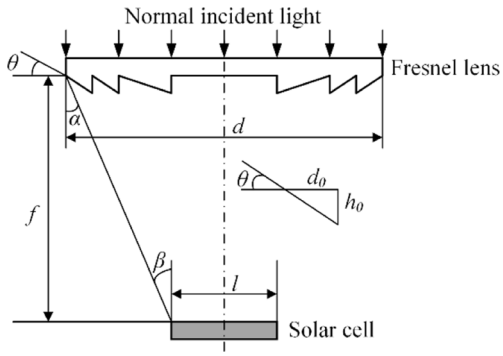

Fig. 3 Optical design of the uniform concentrating Fresnel lens

According to Eq. 4, the larger the aperture angle β of the lens is, the more light is reflected and consequently the lower the optical efficiency is. Thus, d cannot be too large when f is constant. When the light on a groove is totally reflected, the inclined angle of the groove is defined as θ_0. The groove number j_0 can be calculated via Eq. 6. Geometrical concentration ratio (GCR) is defined as the ratio of the lens area S_1 to the solar cell area S_2. The maximum GCR λ_{max} can be calculated via Eq. 7.

$$j_0 = 1 + 2f\tan\left(\sin^{-1}(n\sin\theta_0) - \theta_0\right)/l \tag{6}$$

$$\lambda_{max} = S_1/S_2 = \pi(d/2)^2/\pi(l/2)^2 = {j_0}^2 \tag{7}$$

Photovoltaic silicone rubber is a common lens material. The average refractive index of this silicone rubber is 1.411, and λ_{max} can be described in Eq. 8. As shown in Fig. 4, λ_{max} with a wide range can meet the power generation requirements of CPV.

$$\lambda_{max} = (1.99f/l + 1)^2 \tag{8}$$

2.3 Optimization of diameter *d* and focal length *f*

The theoretical optical efficiency (TOE) and theoretical optical concentrating ratio (TOCR) of the lens are mainly influenced by the diameter d and the focal length f. According to Fresnel formulas, the energy flow reflectivity $R1$ is defined in Eq. 9, in which r is the amplitude reflectivity. Subscripts s and p are the vibration component in the incident plane and the plane perpendicular to the incident plane respectively.

$$R1_s = |r_s|^2, \quad R1_p = |r_p|^2 \tag{9}$$

Based on the law of energy conservation, average transmissivity of energy flow (TEF) T is described in Eq. 10. TEF of the emergent plane is defined as the weighted mean of that of the center circle surface and all grooves. When the incident angle i_1 is 0°, TEF of the incident plane τ_{in} and that of the

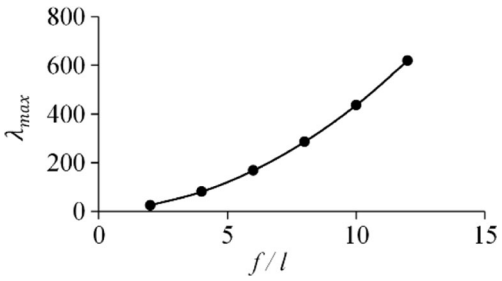

Fig. 4 Relationship between λ_{max} and f/l

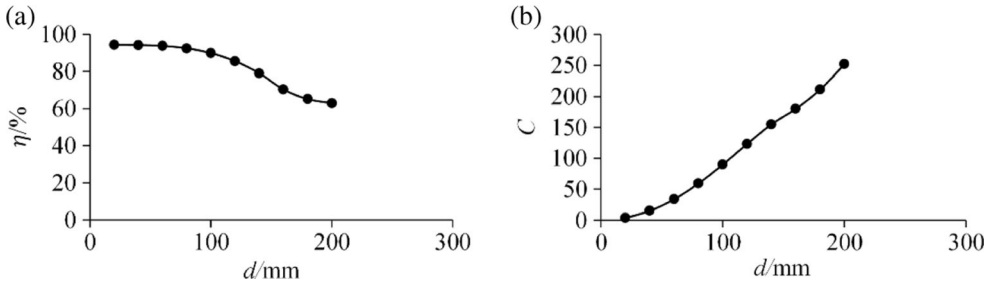

Fig. 5. **a** Relationship between η and d. **b** Relationship between C and d

emergent plane τ_{out} of the lens with equal groove width are described in Eq. 11. τ_j is the TEF of number j groove, which can be calculated by Eq. 10.

$$T = 1-\left(R_{s1} + R_{p1}\right)/2 \tag{10}$$

$$\tau_{in} = 4n/(n+1)^2, \quad \tau_{out} = \left(\sum_{j=2}^{N} \tau_j + \tau_1\right)/N \tag{11}$$

When calculating TOE, only the reflection loss of the incident plane and the emergent plane will be considered, and TOE η of the lens with equal pitch width can be described in Eq. 12. TOCR C is defined as the ratio of the irradiance of the incident plane E_{in} to that of the emergent plane E_{out}. C can be calculated via Eq. 13.

$$\eta = \tau_{in}\tau_{out} \tag{12}$$

$$C = \frac{E_{out}}{E_{in}} = \frac{\eta(d/l)^2 E_{in}}{E_{in}} = \eta\left(\frac{d}{l}\right)^2 \tag{13}$$

In the design specification, the solar cell diameter is 10 mm; the groove width of the lens is 5 mm; the refractive index is 1.411. As shown in Fig. 5, when the focal length f is 150 mm, η decreases and C increases as d increases. Therefore, d cannot be too large for high η. As shown in Fig. 6, when d is 150 mm, η and C both increase as d increases, and when f is more than 150 mm, η and C tend to be a constant.

The design parameters of the lens are optimized as shown in Table 1. η and C are 92.45% and 55.47 respectively. The lens consists of seven grooves, and the maximum and minimum inclined angles of these grooves are 27.627° and 4.662° respectively. Every groove consists of ten sub-grooves. For meeting the requirements of the subsequent uniform concentrating test, l is selected to be 10 mm, and the GCR is relatively small. When a high GCR is needed, d (or l) will be appropriately increased (or decreased).

3 Machining process and experiments of the Fresnel lens mold

3.1 *B* axis rotating machining method

B axis rotating machining method is applied to avoid the tool tip engaged in the cutting process. Thus, a stable cutting process and lower tool wear will be ensured. As shown in Fig. 7, the lens groove consists of a conical and a cylindrical surface. *TB* is the distance between the tool tip and the rotating center of *B* axis. When *TB* is 0, the lens groove can be precisely and efficiently machined with the rotation of *B* axis from position 1 to position2. Before machining, the tool alignment of *B* axis rotation is conducted to make *TB* equal to 0 [15]. As shown in Fig. 8, *B* is the rotating center of *B* axis and *T* is the tool tip. Three different coordinates of the tool tip *T*, T_1, and T_2 are obtained through image recognition technology, and *TB* can be calculated by Eq. 14. Then, the tool is translated quantitatively in the *XZ* plane until *TB* is 0.

As shown in Fig. 9, conventional CNC machining methods are relatively simple, but the tool tip is prone to vibrate. As a result, optical surface may be difficult to be achieved.

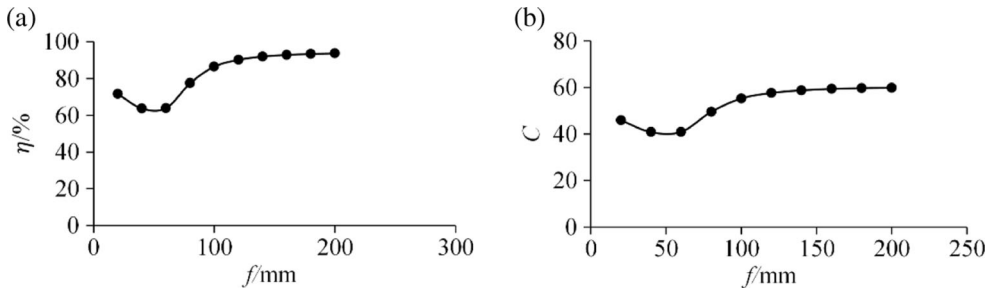

Fig. 6. **a** Relationship between η and f. **b** Relationship between C and f

Table 1 Design parameters of the lens

f	d	l	Groove width	GCR	Lens material	Refractive index
150 mm	80 mm	10 mm	0.5 mm	64	3210 A/B	1.411

Moreover, the tool will wear easily when the cutting edge angle is relatively large. In the proposed B axis rotating machining method, the cutting edge with a certain length instead of the tool tip is engaged in the cutting, so a stable cutting process will be achieved as well as optical surface. Lower tool wear can be also achieved.

$$\begin{aligned} X_B &= \frac{4Z_1\cos^2(\gamma/2) - Z_2}{4\cos(\gamma/2)\sin(\gamma/2)} \\ Z_B &= \frac{4Z_2\cos^2(\gamma/2) - Z_2 - 2Z_1}{4\sin^2(\gamma/2)} \\ TB &= \sqrt{{X_B}^2 + {Z_B}^2} \end{aligned} \tag{14}$$

3.2 Machining path planning and analysis of machining parameters

The V-shaped cutting tool is used, as shown in Fig. 10. The relationship between the cutting edges L_2 and L_3 and the maximum machining length $L_{\max}$, and the relationship between the tool included angle α_T and the minimum machining angle $\alpha_{\min}$ are described in Eq. 15.

As seen from Fig. 11a, before machining, the tool is placed in position 1 where the right cutting edge is parallel to the Z axis, and position 1 is set as the 0 point of B axis rotating machining. If the tool is moved along path ① from position 1 to position 2, and then is rotated to position 3 along path ②, one groove will be machined. When position 1 is far away from (or near to) the cylindrical surface, the machining allowance of the cylindrical surface (or the conical surface) is large, which will decrease the machining stability.

$$\alpha_{\min} > \alpha_T, \quad L_{\max} < L_2 = L_3 \tag{15}$$

To increase the machining stability, the cutting path shown in Fig. 11b, c is applied. In Fig. 11b, the tool is moved along path ① from the middle point of the groove (position 1) to position 2, and then is rotated along path ② from position 2 to position 3 to machine the cylindrical surface. Then, as shown in Fig. 11c, the tool is rotated along path ③ from position 3 to position 4 to machine the conical surface. The process is repeated until all grooves are machined. When machining pitches, the relationship among the inclined angle of feeding α_1, the machining angle of a conical surface α_2, the tool included angle α_T, and the machining angle of a groove α_0 is described in Eq. 16. Finally, as seen from Fig. 11c, a round tool on another tool holder is moved along path ④ to machine the center circle surface.

$$\alpha_1 + \alpha_2 + \alpha_T = \alpha_0 \tag{16}$$

As shown in Fig. 11b, when the tool is moved from position 1 to position 2, the tool tip will first enter into the workpiece, and the cutting force increases gradually. To prevent the brittle tool tip from serious wear or fracture, a small feed rate is selected. During the tool rotation from position 2 to position 3, the cutting volume increases gradually. The tool bears a variable load, so small feed rate is preferred for a stable cutting process. The relationship among the rotating speed of B axis F_B (°/min), the feed rate F (mm/min), and the distance between the tool tip and the cutting point R (mm) is described in Eq. 17. In practical machining, the rotating speed of B axis is set. As shown in Fig. 11c, during the tool rotation from position 3 to position 4, the tool also bears a variable load, and a small feed rate is preferred. When the round tool with high rigidity is used, the cutting fore is relatively small, so a larger feed rate is selected.

$$F = \frac{\pi R F_B}{180} \tag{17}$$

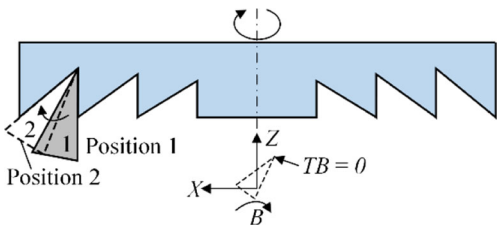

Fig. 7. B axis rotating machining method.

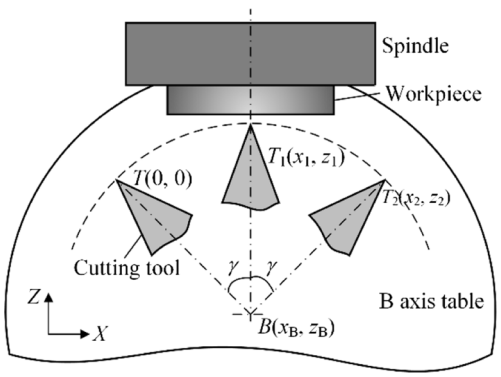

Fig. 8 Schematic of B axis tool alignment method

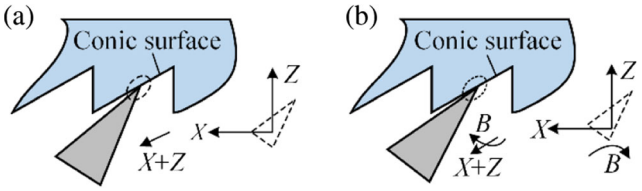

Fig. 9 Conventional CNC machining methods: **a** tool tip engaged in the cutting and **b** constant cutting edge angle in cutting process

Aluminum alloy with good plasticity is selected as the workpiece material. Burrs are easily induced when cutting this material. As seen from Fig. 11, the cylindrical surface is nearer to the center line of the spindle than the conical surface. When machining the cylindrical surface, the cutting speed is smaller than that of machining the conical surface, and decreases gradually in the machining process. Therefore, the cutting force is larger than that of machining the conical surface, leading to the plastic deformation of the workpiece easily. The plastic deformation is the main cause of burrs. To prevent burrs, the rotating speed of *B* axis and the spindle speed will be decreased and increased respectively. When machining the conical surface, the cutting speed increases gradually in the machining process, which helps to decrease the cutting force. As a result, burrs are difficult to form. Based on the above analysis, the cutting path planning is that the outmost groove is first machined and then the near groove in turn, and finally the innermost groove. In the machining process, burrs induced by machining the cylindrical surface will be removed when machining of the conical surface later.

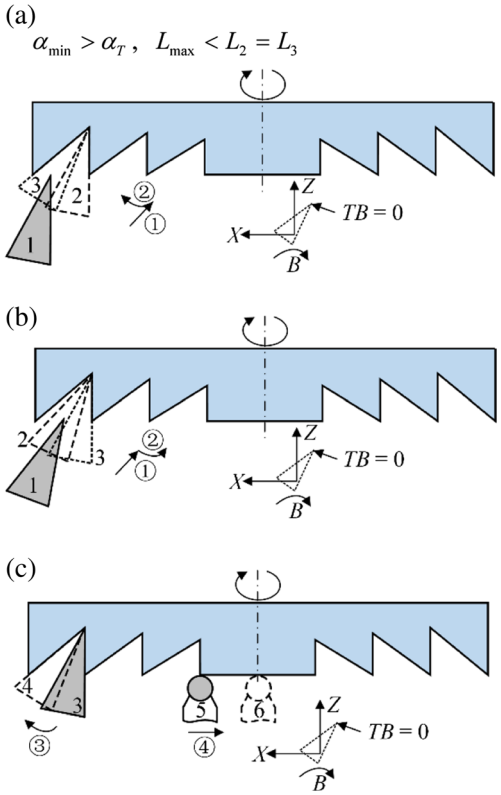

Fig. 11 Cutting path planning: **a** vertical feeding, **b** machining the conical surface through the feeding with an inclined angle, and **c** machining the cylindrical surface and the center circle surface

3.3 Machining experiments and discussion

The technical specifications of the typical Fresnel lens mold in China are as follows: the top and the bottom of the mold groove with sharp corner must be achieved, the diameter of the sharp corner of the mold groove is no greater than 10 μm, the width and height accuracy of the mold groove is better than 1.5 μm, and the surface roughness *S*a of the working surface of the mold is better than 20 nm.

Figure 12 shows the machining experimental setup of ultra-precision cutting. The resolution of *X* axis and *Z* axis is 5 nm. The straightness of the aerostatic linear guides is 0.15 μm/200 mm. The resolution and division accuracy of *B* axis are 0.036″ and 0.3″ respectively. The camera is used to obtain coordinates of the tool during the tool alignment of *B* axis rotation.

The machining path planning and machining parameters are to be optimized through cutting tests to prevent burrs, sharp corner defects, or surface scratches. Thus, better machining accuracy and optical surface will be achieved. The diameter of the workpiece and the lens mold is 100 and 80 mm respectively. The single-point diamond V-shaped tool with a 60° included angle is selected, of which the nose radius is less than 1 μm. The single-point diamond round tool with a nose radius of 2 mm is used. To verify the influence of cutting

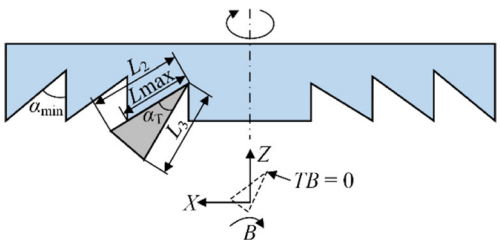

Fig. 10 Specification of the V-shaped cutting tool

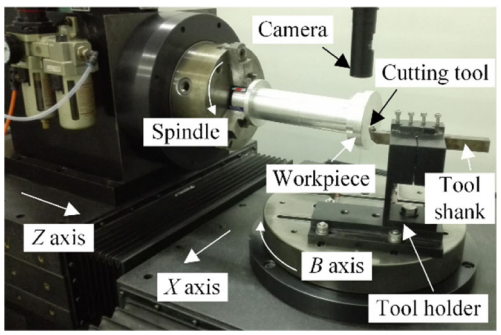

Fig. 12 Machining experimental setup of ultra-precision cutting

path on burr formation, workpiece 1 is first machined. The cutting path is that the innermost groove is first machined and finally the outmost one, and every groove is machined by one cut. When machining a groove, the machining strategy of rough and then finish cutting is applied. The rough cutting is conducted until the remaining machining angle is 0.1°, and the *B* axis rotating speed is 50 deg/min. Then, the finish cutting is conducted, and the *B* axis rotating speed is 3 deg/min. The spindle speed is 800 rpm, and the inclined angle feeding speed is 1 mm/min. The cutting parameters for the center plane are that the spindle speed is 800 rpm and the feeding speed is 5 mm/min. Kerosene mist is used as the cutting fluid.

Figure 13a–c shows the machining results of workpiece 1. Obvious burrs with an average length of 6 μm can be observed on the sharp corners, as well as obvious scratches on the machined surface. To eliminate the results caused by accidental factors and the blunting cutting edge, workpiece 2 is machined by a new tool. The similar results are shown in Fig. 13d–f, by which the influence of cutting path on burr formation is verified. The cutting burrs decrease the form accuracy of the mold, and the scratches on the machined surface lower the surface quality, which lowers the optical performance of the lens. Therefore, it is necessary to prevent the cutting burrs and scratches.

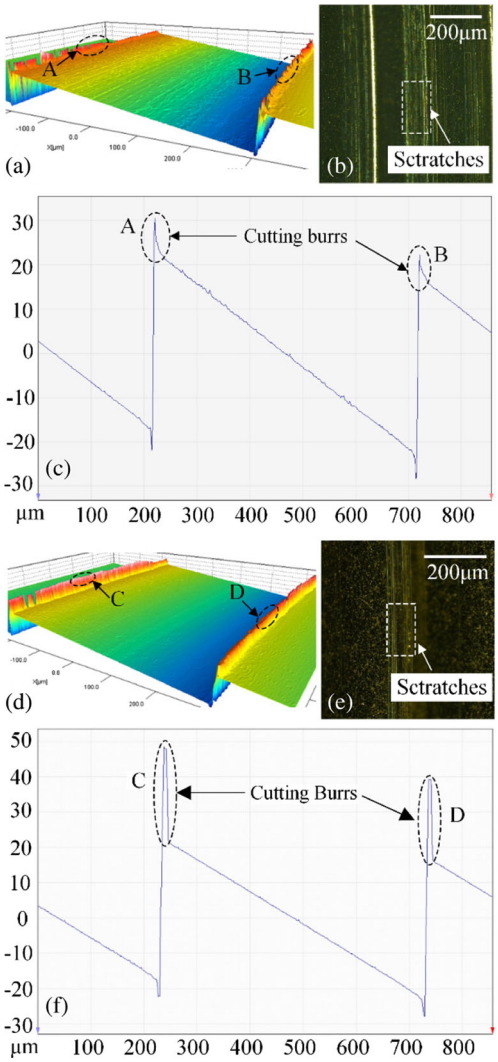

Fig. 13 Experimental results of the first machining. Workpiece 1: **a** obvious burrs on the sharp corners (in three dimension), **b** obvious scratches on the machined surface, and **c** obvious burrs (in two dimension). Workpiece 2: **d** obvious burrs on the sharp corners (in three dimension), **e** obvious scratches on the machined surface, and **f** obvious burrs (in two dimension)

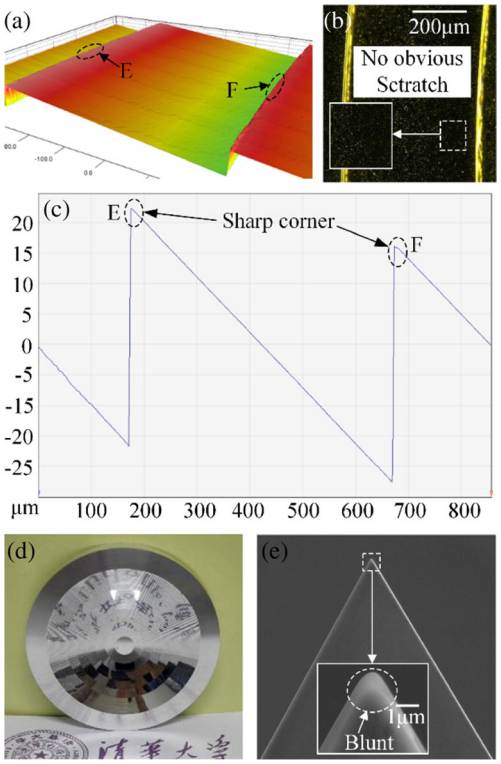

Fig. 14 Experimental results of the second machining: **a** no obvious burrs (in three dimension), **b** no scratches on the machined surface, **c** no obvious burrs (in two dimension), **d** lens mold, and **e** slightly blunt tool

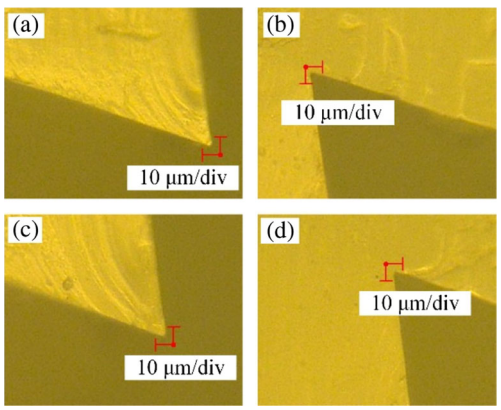

Fig. 15 Silicone rubber grooves cast by the mold in Fig. 14: **a** top corner of the first groove, **b** bottom corner of the first groove, **c** top corner of the second groove, and **d** bottom corner of the second groove

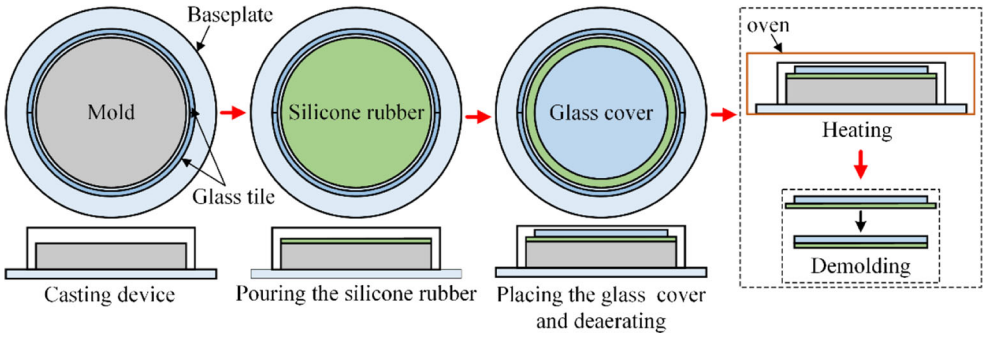

Fig. 16 Preparation process of the silicone rubber lens

Because the groove is machined by one cut with a large machining allowance, the cutting force is large. Therefore, the plastic deformation of workpiece can easily occur, leading to the formation of cutting burrs. When the machining allowance is large, continuous chips are observed and these chips will scratch the machined surface. Based on this analysis, the optimal cutting path is that the outmost groove is first machined and then the near groove one by one until the innermost groove is machined. Every groove is machined by two cuts with the second cutting depth of 10 μm. The spindle speed is increased to 1000 rpm.

In the second machining experiment, the same tool in the first machining experiment is used. As seen from Fig. 14, the mold without cutting burrs and scratches is achieved. After machining three workpieces, the tool is slightly blunt, which can be further prevented by more than two cuts. The surface roughness *Sa* and the dimensional accuracy of the mold are measured by Phase Shift MicroXAM-3D. The average width accuracy of the mold groove is 0.94 μm, the average height accuracy of the mold groove is 0.43 μm, and the average surface roughness *Sa* of the mold is 11.73 nm. As shown in Fig. 15, the diameter of the sharp corner of the mold groove is less than 10 μm. The results verify the feasibility of the *B* axis rotating machining process.

4 Concentrating uniformity test

4.1 Preparation of silicone Fresnel lens

The lens material is 3210 A/B silicone rubber which is suitable for casting. As shown in Fig. 16, the mold is placed on a circular glass plate. The silicone rubber is slowly poured into the mold. Then, a quartz glass cover is slowly placed on the silicone rubber. Two glass tiles encircle the mold to prevent the glass cover from sliding. The whole casting device is put into an oven with a heating temperature of 100 °C for 10 min and then taken out. The lens bonding with the glass cover is released from the mold, and a silicone rubber lens with a thickness of about 0.7 mm is obtained. As shown in Fig. 17, only several bubbles are observed in the lens without sharp corner defects.

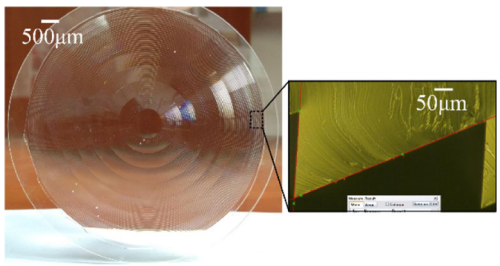

Fig. 17 Silicone rubber Fresnel lens

4.2 Test method

The light passing through the lens will be expectedly focused on a circular facula with a diameter of 10 mm. In the facula, the irradiance of all points is theoretically the same, resulting in the same temperature of every point. Thus, the concentrating uniformity can be evaluated indirectly by the temperature uniformity of the facula. As seen from Fig. 18, certain thermal resistances are used to measure the temperature of specific positions. T_i is defined as the temperature of number i thermal resistance. N is the total number of thermal resistances. u_T is defined as the temperature uniformity, and u_T can be calculated by Eq. 18. T_{max} and T_{min} are the biggest and the smallest

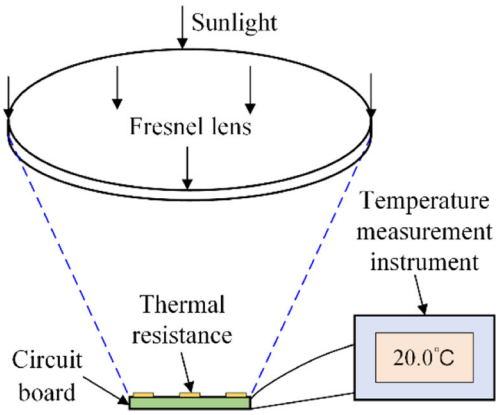

Fig. 18 Concentrating uniformity test method

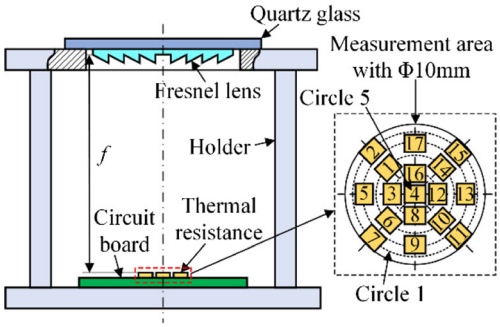

Fig. 19 Concentrating setup and distribution of thermal resistances

temperatures respectively. The bigger u_T is, the better the concentrating uniformity is.

$$u_T = 1 - \frac{T_{max} - T_{min}}{T_{max} + T_{min}} \tag{18}$$

4.3 Test results and discussion

As seen from Fig. 19, the distance between the lens and the thermal resistance is the focal length *f*. The outmost measurement circle is numbered 1, and the innermost one is numbered 5 in turn.

PT1000 SMD-V 0603 is selected as the thermal resistance, of which the measurement range is from − 50 to + 130 °C, temperature tolerance is ± 0.24%, and the package size is 1.6 mm × 0.8 mm. Thermal resistances as many as possible should be placed in the concentrating facula to achieve accurate measurements, and 17 thermal resistances are distributed in five measurement circles. All resistances are numbered. The measurement instrument can simultaneously record the temperature of 18 thermal resistances, and its measurement accuracy is ± 0.5 °C.

Total ten measurements are conducted at noon. As seen from Fig. 20, the concentrating facula coincides with the measurement area with a diameter of 10 mm, meeting the design requirement. In all ten measurements, three measurements are valid. The average temperature of the three valid measurements is shown in Fig. 21. The center

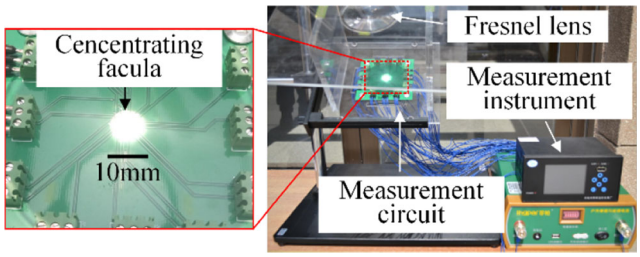

Fig. 20 Concentrating uniformity test setup and concentrating effect

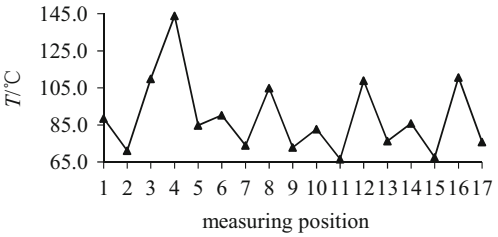

Fig. 21 Average temperature of different positions of the three valid measurements

number 4 position bears the highest temperature of 143.9 °C, while number 11 position is the lowest. The temperature uniformity of five measurement circles is shown in Fig. 22. When calculating u_T by Eq. 18, T_{max} and T_{min} are the biggest and the smallest temperatures of the average temperature of the measurement circle and all measurement circle respectively. The temperature uniformity of number 1 circle to number 4 circle is better than 87%.

Because the distribution density of the resistances is bigger and the heat dissipation condition is worse near to the center position of the concentrating facula, the temperature of the center number 4 position is obviously higher than that of other positions. As a result, the temperature of number 4 position is inaccurate and higher than that in the real one. When calculating the temperature uniformity of the whole concentrating facula, all the other 16 measurements will be used except the temperature of number 4 position. According to Eq. 18, the temperature uniformity of the whole concentrating facula is 75.2%.

The designed uniform concentrating Fresnel lens achieves a certain concentrating uniformity. By investigation into the geometrical structure of the lens, the concentrating surface is conical surface of which the concentrating characteristic is similar to that of spherical surface. Thus, the light passing through the conical surface will not be concentrated uniformly in an area with a specific diameter, but concentrated near to the center, resulting in larger irradiance and thus higher temperature of the center area. In further research, the optimized geometrical design of the lens, such as the groove width and the inclined angle of the grooves, will be conducted for a better concentrating uniformity.

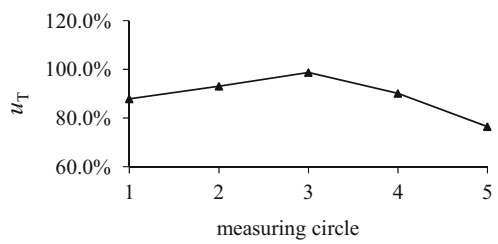

Fig. 22 Temperature uniformity of different measurement circles

5 Conclusion

To increase the photoelectric conversion efficiency of CPV systems, a design of uniform concentrating Fresnel lens was proposed, and a *B* axis rotating machining process of its mold was developed. The mold machining experiments and the concentrating uniformity test of the lens were carried out, and the results verified the feasibility of the uniform concentrating design and the *B* axis rotating machining process. The conclusions can be drawn as follows:

(1) The concentrating planes of the Fresnel lens were designed to be conical ones, so the light passing through these conical planes can be superposed on the same position, and finally, a uniform concentrating circular facula was achieved. By analyzing the factors influencing the theoretical optical efficiency and optical concentrating ratio of the lens, the diameter and the focal length were optimized. A uniform concentrating Fresnel lens with a diameter of 80 mm, a focal length of 150 mm, and a concentrating facula with a diameter of 10 mm were designed, and its theoretical optical efficiency was 92.45%.

(2) The formation of cutting burrs and scratches on the machined surface of the molds was mainly influenced by the machining path, cutting speed, *B* axis rotating speed, and cutting depth. Tests of these factors were carried out to optimize the cutting path planning and machining parameters. The optimal machining strategy was that the outmost groove was first machined and then the near groove one by one until the innermost groove was machined. Every groove was machined by two cuts with the second depth of cut of 10 μm. Under a maximum *B* axis rotating speed of 50 deg/min, the uniform concentrating lens mold was machined with dimensional accuracy of 1.0 μm and surface roughness better than 13 nm.

(3) A silicone rubber Fresnel lens with no sharp corner defects was cast based on the uniform concentrating lens mold. A concentrating uniformity test setup was designed to measure the temperature uniformity of this lens, and the concentrating uniformity of Fresnel lens was evaluated by the temperature uniformity. The concentrating uniformity of the lens was better than 75%. In further research, the optimal geometrical design of the lens will be conducted for a better concentrating uniformity.

Acknowledgements We thank Wacker Chemicals (China) Co., Ltd. for providing the silicone rubber, and Shanghai Superhard Precision Tools Co., Ltd. for diamond tool customization service.

Funding information This research is supported by the Beijing Natural Science Foundation (No. 3131003, No. 3172013), Independent Research Project of the State Key Laboratory of Tribology at Tsinghua University (No. SKLT2013C01), and National Natural Science Foundation of China (No. 51675054).

References

1. Xie WT, Dai YJ, Wang RZ, Sumathy K (2011) Concentrated solar energy applications using Fresnel lenses: a review. Renew Sust Energ Rev 15(6):2588–2606. https://doi.org/10.1016/j.rser.2011.03.031
2. Scanlon W (2014) NREL Demonstrates 45.7% Efficiency for Concentrator Solar Cell. NREL Official Website. http://www.nrel.gov/news/press/2014/15436. Accessed 16 Dec 2014
3. Garca I, Algora C, Stolle IR, Galiana B (2008) Study of non-uniform light profiles on high concentration III–V solar cells using quasi-3D distributed models. Proc 33rd IEEE Photovoltaic Specialist Conference: 1–6. https://doi.org/10.1109/PVSC.2008.4922908
4. Katz EA, Gordon JM, Feuermann D (2006) Effects of ultra-high flux and intensity distribution in multi-junction solar cells. Prog Photovolt Res Appl 14(4):297–303. https://doi.org/10.1002/pip.670
5. Victoria M, Domínguez C, Antón I, Sala G (2009) Comparative analysis of different secondary optical elements for aspheric primary lenses. Opt Express 17(8):6487–6492. https://doi.org/10.1364/OE.17.006487
6. Benítez P, Miñano JC, Zamora P, Mohedano R, Cvetkovic A, Buljan M, Chaves J, Hernández M (2010) High performance Fresnel-based photovoltaic concentrator. Opt Express 18(S1):A25–A40. https://doi.org/10.1364/OE.18.0000A25
7. Pan JW, Huang JY (2011) High concentration and homogenized Fresnel lens without secondary optics element. Opt Commun 284(19):4283–4288. https://doi.org/10.1016/j.optcom.2011.06.019
8. Wang G, Chen ZS, H P, Cheng XF, Mo SP, Jiang SL (2012) Research on strip-focus Fresnel solar concentrator with regular illumination. Acta energiae soaris sinica 5:1–7 (in Chinese)
9. Yan JW, Zhang ZY, Kuriyagawa T, Gonda H (2010) Fabricating micro-structured surface by using single-crystalline diamond endmill. Int J Adv Manuf Technol 51(9–12):957–964. https://doi.org/10.1007/s00170-010-2695-2
10. Brinksmeier E, Ralf G, Lars S (2012) Review on diamond-machining processes for the generation of functional surface structures. CIRP J Manuf Sci Technol 5(1):1–7. https://doi.org/10.1016/j.cirpj.2011.10.003
11. Yan JW, Maekawa K, Tamaki J, Kuriyagawa T (2005) Micro grooving on single-crystal germanium for infrared Fresnel lenses. J Micromech Microeng 15(10):1925–1931. https://doi.org/10.1088/0960-1317/15/10/019
12. Fan YF, Zhu YJ, Pan WQ (2010) Ultra-precision cutting of Fresnel lenses on single crystal germanium and the machining processing analysis. Proc SPIE 7655:207–208. https://doi.org/10.1117/12.866709
13. Allsop JL, Mateboera A, Shorea P (2011) Optimising efficiency in diamond turned Fresnel mould masters. Proc SPIE 8065:170–187. https://doi.org/10.1117/12.882925
14. Wang YL, Zhao QL, Shang YJ, Lv PX, Guo B, Zhao LL (2011) Ultra-precision machining of Fresnel microstructure on die steel using single crystal diamond tool. J Mater Process Technol 211(12):2152–2159. https://doi.org/10.1016/j.jmatprotec.2011.07.018
15. Duong CV, Li CJ, Li Y, Gao X (2014) Tool alignment on the *B* axis rotary table of an ultra-precision lathe machine. J Tsinghua Univ (Sci Technol) 54:1466–1470 (in Chinese). https://doi.org/10.16511/j.cnki.qhdxxb.2014.11.005
16. Li CJ, Li Y, Gao X, Duong CV (2015) Ultra-precision machining of Fresnel lens mould by single point diamond turning based on axis *B* rotation. Int J Adv Manuf Technol 77(5–8):907–913. https://doi.org/10.1007/s00170-014-6522-z
17. Davies MA, Evans CJ, Bergner BC (2003) Application of precision diamond machining to the manufacture of microphotonics components. Proc SPIE 5183:94–108. https://doi.org/10.1117/12.506373